J Solid State Electrochem (2016) 20:459–468
DOI 10.1007/s10008-015-3058-6

ORIGINAL PAPER

Electrochemical synthesis of ZnO nanorods/porous silicon composites and their gas-sensing properties at room temperature

Dali Yan[1] · Shenyu Li[2] · Shiyu Liu[1] · Ming Tan[3] · Dejun Li[1] · Yun Zhu[1]

Received: 2 July 2015 / Revised: 10 October 2015 / Accepted: 14 October 2015 / Published online: 31 October 2015

Abstract The zinc oxide (ZnO) nanorods with different aspect ratio (length/diameter) were grown directly on the porous silicon (PS) substrate through electrochemical synthesis. The obtained ZnO nanorods/PS products were investigated by scanning electron microscopy (SEM), transmission electron microscopy (TEM), X-ray diffraction (XRD), and gas-sensing test. Comparative study shows that the addition of nonionic polymer polyvinylpyrrolidone (PVP) into oxygenated zinc chloride electrolyte can modulate the crystal growth and the aspect ratio of ZnO nanorods from electrodeposition, thus, influence the gas-sensing properties of ZnO nanorods/PS composites. With appropriate amount of PVP in the electrolyte, the product possessing high-density and large aspect ratio ZnO nanorods has an obvious improvement of the NO_2-sensing performances with high sensitivity, fast response-recovery characteristic, and good repeatability and selectivity. The gas-sensing mechanism was discussed in the paper. The result indicated that the heterojunction effect of ZnO nanorods and PS may be responsible for the excellent gas-sensing properties.

Keywords Zinc oxide nanorods · Porous silicon · Electrochemical synthesis · Gas-sensing properties

✉ Dali Yan
freeyandali@163.com

[1] College of Physics and Materials Science, Tianjin Normal University, Tianjin 300387, China

[2] Schools of Marine Science and Engineering, Hebei University of Technology, Tianjin 300130, China

[3] Department of Physics, College of Sciences, Tianjin University of Science & Technology, Tianjin 300457, China

Introduction

Over the past few decades, air pollution problems have become more and more serious. In particular, nitrogen dioxide (NO_2) which results from combustion and automotive emissions is one of the most toxic gases in the atmosphere and is responsible for the formation of acid rain and photochemical smog [1]. Therefore, the detection of NO_2 gas is a crucial point for the environmental protection and human health. The development of NO_2 gas sensor has attracted intensive attention [2]. So far, several kinds of solid-state sensors have been developed, including the solid-state potentiometric gas sensors [3, 4], resistive types gas sensors [1, 2], and capacitive types gas sensors [5]. The solid-state potentiometric gas sensor is based on the generation of voltage and currents in potentiometric cells using solid electrolytes such as the various zirconia-based materials [3, 4, 6]. Some mixed potential zirconia-based gas sensors can exhibit excellent NO_2-sensing performances in oxygen containing humid atmospheres at high temperatures and show great application value for automotive and combustion industries [3]. However, in the gas-sensitive detection at lower temperature and even at room temperature, semiconductor resistive-type gas sensors have great development potentials.

Zinc oxide (ZnO) as a wide direct band gap semiconductor (E_g = 3.37 eV) has been extensively investigated due to its wide application in many fields including gas sensors [7], optoelectronic devices [8], and photovoltaic devices [9]. With the advantages of the high surface to volume ratio and electron mobility, ZnO nanostructures with various shapes such as nanorods, nanowires, nanobelts, and nanosheets have been evaluated as a competitive candidate for detecting many gases such as NO_2, H_2, CO, and ethanol [10–13]. The relevant studies have shown that the gas-sensing properties of ZnO nanocrystals were strongly dependent on many factors

including the morphology [13, 14], size [15], crystal defect [16] and even crystal density. Unfortunately, because of the high reaction activation energy with gas molecules, ZnO-based gas sensors usually have a high working temperature above 150 °C [11]. It is unfavorable for device integration and energy conservation. So the practical application of ZnO-based gas sensor is hampered. On the other hand, ZnO nanocrystals with various shapes have been synthesized using a variety of technologies, including thermal evaporation [17], solvothermal [18, 19], sol-gel [20], and electrochemical synthesis [21, 22]. The preparation of ZnO films using electrochemical synthesis presents several advantages such as relatively high deposition rate, low deposition temperature, and low equipment cost. Sometimes, polymers are employed in electrolyte to control the nucleation, growth, and alignment of crystals [23].

Porous silicon (PS) as a micro-nanostructure silicon material, with the characteristics of a large specific surface area and surface chemical activity, has been used for detecting many gases, NO_2, NH_3, H_2S, H_2, ethanol, and so on [5, 24, 25]. There are many advantages in the use of PS for gas detection. Firstly, PS shows gas-sensing properties at relatively low temperatures, even at room temperature (RT), in contrast to the high working temperature of the traditional metal oxide gas-sensing material [26]. Secondly, the gas sensor based on PS is compatible with silicon IC technology, which is beneficial to the miniaturization and integration of the gas sensor. What is more, PS could be produced simply and at low cost by chemical etching of silicon in HF solution. But the disadvantages of low sensitivity and the thermal stability limit its applications [26, 27].

To overcome the shortcomings of ZnO and PS for gas sensing, ZnO nanorods were supported on the PS substrate to build composite gas-sensing materials. It may be beneficial in reducing operating temperature and enhancing gas sensitivity for their heterojunction effect. To the best of our knowledge, studies in this area are not a lot [27, 28].

In this paper, large-scale ZnO nanorods with different aspect ratio (length/diameter) were grown onto porous silicon substrate through a simple and low-temperature electrochemical synthesis method. The poly(vinylpyrrolidone) (PVP) was added into the electrolyte to modulate the growth of ZnO nanocrystals. The gas-sensing characterization of ZnO nanorods/PS composites at room temperature were reported which indicated the composite with high-density and large aspect ratio ZnO nanorods may have great potential for application in low power consumption sensors.

Experimental

The schematic diagram for synthesis of ZnO nanorods/PS composite was shown in Fig. 1.

Synthesis and characterization of ZnO nanorods/PS composite

The PS substrates were prepared by galvanostatic electrochemical etching of p-type silicon wafer with the resistivity 10–15 Ω cm and (100) orientation in a Teflon double-tank cell configuration [29] (step 1 in Fig. 1). The double-tank cell contains the electrolyte, which was composed of 1:2 volume ratios between HF (hydrofluoric acid) and DMF (*N*,*N*-dimethyl formamide). A pair of platinum (Pt) electrodes was immersed into the electrolyte of each half-cell used as the anode and cathode, respectively, just as shown in Fig. 2. The etching current density and etching time were 100 mA cm^{-2} and 6 min, respectively. Immediately after etching, the as-prepared PS were rinsed with deionized water and then stored in ethanol.

Hydrofluoric acid is one of the most corrosive acids. Be cautious of safety during using this product. Hydrofluoric acid exposure requires immediate specific and specialized medical treatment.

For the sake of electrodeposition on the semiconductor PS, a layer of Pt film about 100 nm was deposited on the rear of the PS substrate by magnetron sputtering to form a good ohmic contact (step 2 in Fig. 1). It makes sure the electrodeposition potential drop in the activity area of PS rather than contact interface. The electrode lead was extracted from the Pt films and sealed with silica gel layer for waterproof (step 3 in Fig. 1). Then the PS was immersed in a HF solution within 1 min for SiO_2 layer removal and H-terminated surface formation, followed by rinsing with deionized water. The as-obtained samples were used for electrodeposition immediately.

The electrochemical deposition of ZnO was carried out potentiostatically at −0.9 V (vs. SCE) for 1 h, in an O_2-saturated aqueous solution of 0.005 M of $ZnCl_2$ and 0.1 M of KCl maintained at 65 °C (step 4 in Fig. 1). Figure 3 shows the schematic diagram of electrochemical deposition of ZnO nanorods onto PS. A three-electrode electrochemical cell equipped with a magnetic stirrer and a temperature control unit was used for the electrodeposition. The PS substrate, a Pt net, and a saturated calomel electrode (SCE) were used as the working electrode, the counter electrode, and the reference electrode, respectively. The electrolyte was saturated with O_2 by an air pump.

To study the influence of the PVP in the electrolyte on the crystal growth, 3 mass percent concentrations of PVP (0.0, 0.5, and 1.0 %) were added in the electrolyte containing 0.005 M of $ZnCl_2$ and 0.1 M of KCl. The mixed solutions were stirred by the magnetic stirring to dissolve PVP thoroughly. The obtained ZnO/PS products were named S1, S2, and S3, respectively.

The morphologies and structures of the products were investigated by field emission scanning electron microscope

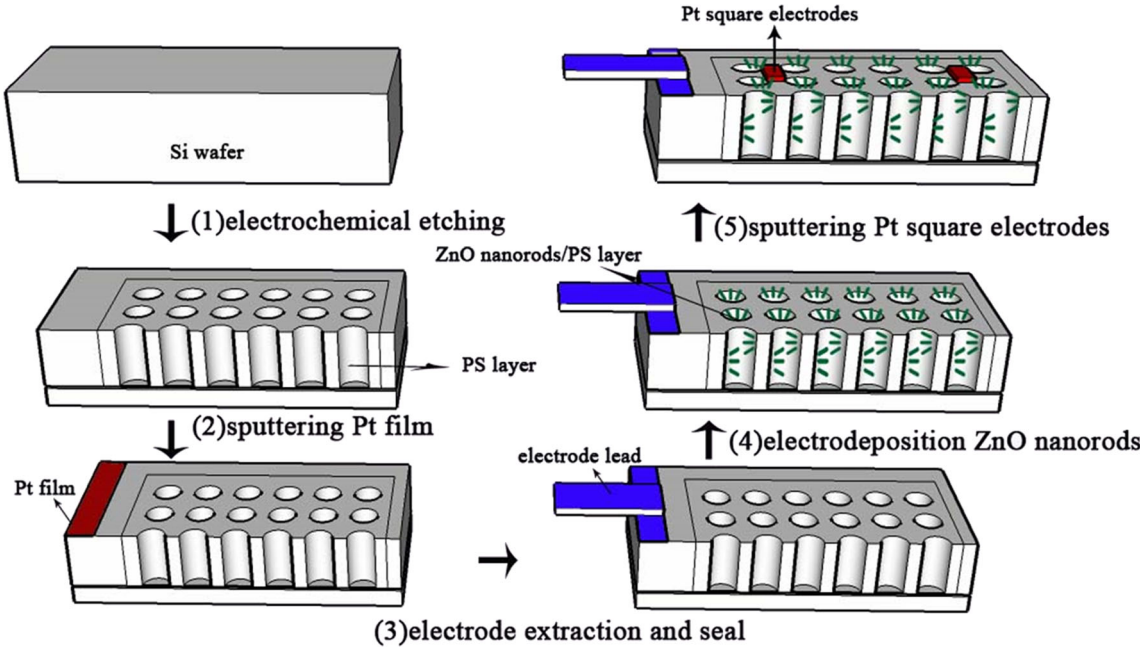

Fig. 1 The schematic diagram for synthesis of ZnO nanorods/PS composite

(FESEM, FEI Nanosem 430; Hitachi S-4800), transmission electron microscope (TEM, JEM100CXII) equipped with selected area electron diffraction (SAED), and X-ray powder diffractometer with CuKα radiation (XRD, RIGAKUD/MAX 2500V/PC).

Gas sensor preparation and measurement

Two Pt square electrodes were deposited on the top of samples by magnetron sputtering using a shadow-making process to fabricate gas sensor (step 5 in Fig. 1).

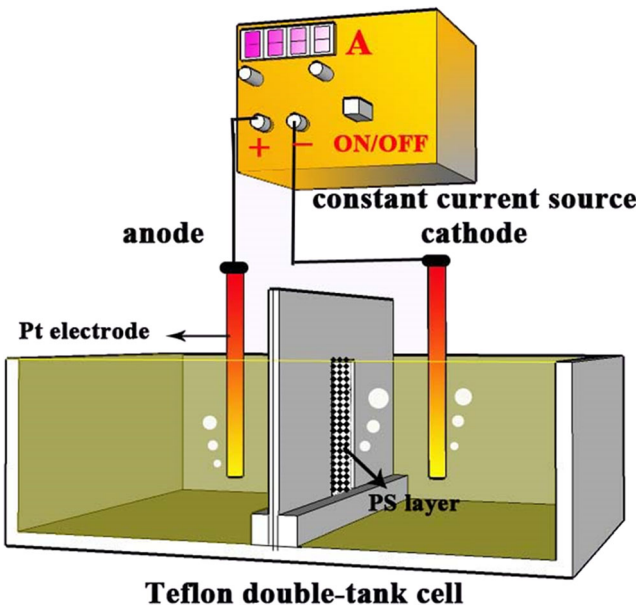

Fig. 2 The schematic diagram of the electrochemical etching

The gas-sensing characteristics of the sensors were evaluated by measuring the resistance changes between the two Pt square electrodes during exposure to certain concentrations of target gas. The measurements were carried out in a static gas-sensing testing system as showed in Fig. 4. The PS-based sensor was placed on a flat heating plate which was fixed in the 30 L sealed testing chamber. The operating temperature of the sensor can be changed by adjusting the temperature controller connected with the heating plate. The resistance of the sensor was detected by a professional digital multimeter (UNI-T UT70D) which was connected to the PC and was used for continuously recording the resistance changes of the sensor. The sampling interval was set to 1 s. In addition, a digital

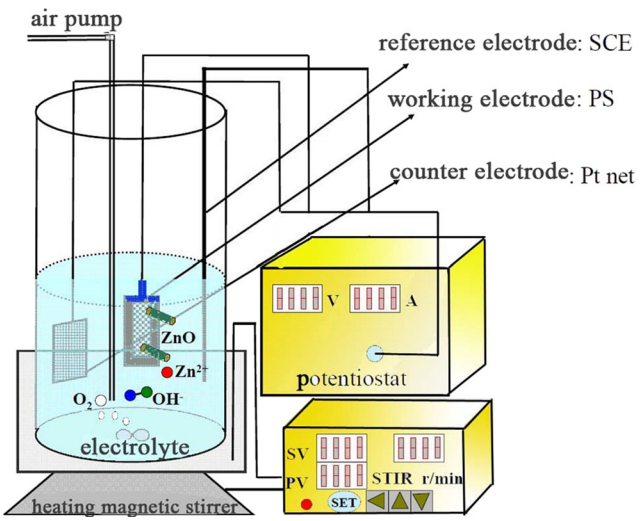

Fig. 3 The schematic diagram of electrochemical deposition of ZnO nanorods onto PS

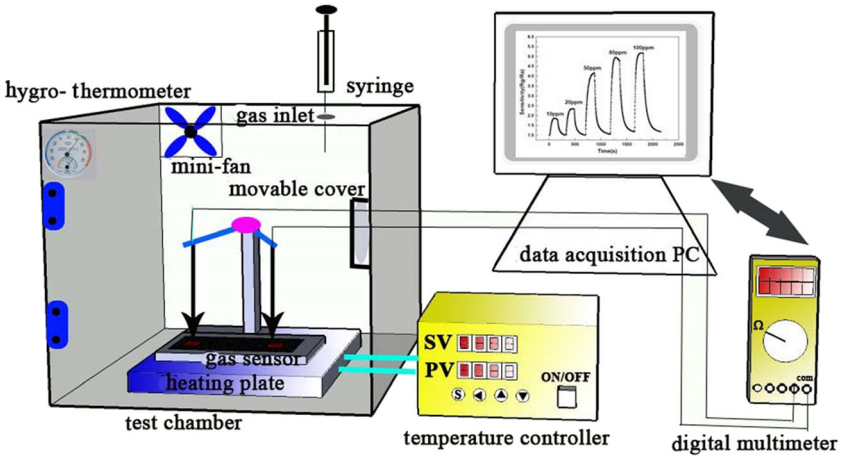

Fig. 4 The schematic diagram of the gas-sensing test system

thermohygrograph was fixed inside the chamber to monitor the ambient temperature and the humidity of the test chamber. Due to influence of humidity on the gas-sensing properties of PS [30], the gas-sensing test was conducted under the condition at the relative humidity (40 % RH) using a dehumidifier. All the sensors (samples PS, S1, S2, and S3) towards 1 ppm NO_2 were measured at different operating temperatures ranging from RT (~25 °C) to 125 °C by adjusting the temperature controller of the heating plate. In this work, each sample was tested at least three times to guarantee the reliability of testing data.

In test, the target gas for the desired concentration was injected into the test chamber by a syringe and spread out quickly under the effect of the blowing mini-fan fixed at the top of the chamber. The resistance of the sensor would response and gradually stabilizes in

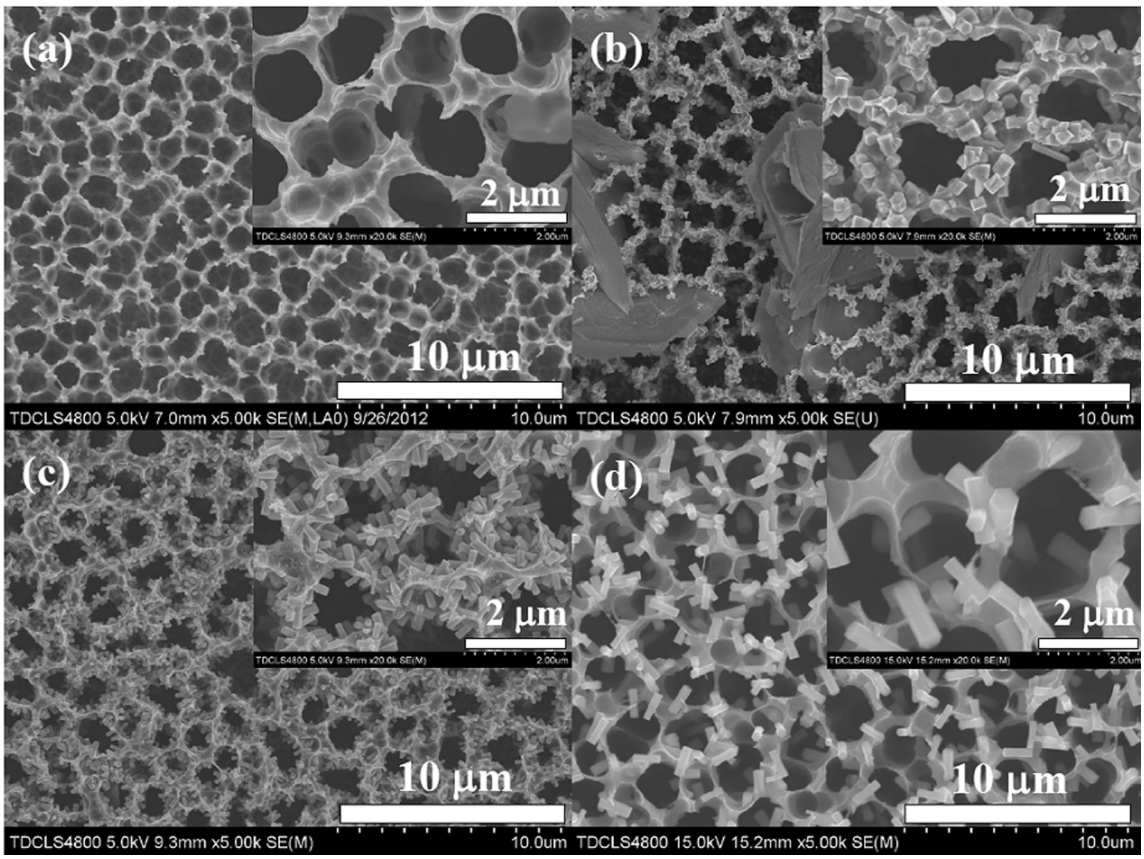

Fig. 5 The top-view SEM images of PS and ZnO nanorods/PS composites: **a** PS, **b** sample S1, **c** sample S2, **d** sample S3. The inset in (**a**–**d**) are the high magnification SEM images of the corresponding products

the target gas atmospheres. Then the movable cover of the chamber was opened and the target gas dissipated rapidly. Meanwhile, the resistance of the sensor recovered in the atmospheric environment.

The sensor sensitivity (or response) was defined as R_a/R_g for oxidizing gas (such as NO_2, etc.) and R_g/R_a for reducing gas (such as NH_3, H_2S, etc.), where R_g and R_a are the resistances of the sensor in target gas and in air, respectively.

Results and discussion

Structural characterization

The top view SEM images of PS and as-synthesized ZnO nanorods/PS composites (sample S1, S2, and S3) were shown in Fig. 5. The cross-sectional view SEM images of the ZnO nanorods/PS (sample S3) and the TEM image of the ZnO nanorods/PS (sample S2) were shown in Fig. 6.

As can be seen from Figs. 5a and 6a, the as-fabricated PS possesses an orderly and uniform distribution of pores with the thickness in the range of 5–8 μm, average aperture about 1.5 μm. According to the IUPAC standard, it is classified into macro-PS based on its pore diameter.

The top-views of potentiostatic deposition ZnO nanorods onto PS with the different concentrations of PVP (sample S1, S2, and S3) were illustrated in Fig. 5b–d, which indicates that the concentration of PVP has a significant effect on the growth of ZnO nanorods.

When the ZnO nanorods were grown from zinc chloride solutions without PVP (sample S1), as shown in Fig. 5b, stubby and overlapping ZnO nanorods covered the porous silicon wafer. The diameter of the hexagonal faces is about 200 nm and the length of the prisms is no longer than 300 nm. The nanorods were very short relative to the diameter with the aspect ratio of about 1–1.5. If the electrolyte was added with 0.5 % PVP (sample S2), as shown in Fig. 5c, the significantly elongated ZnO nanorods densely grow on the surface of the PS with random orientation. The synthesized ZnO nanorods exhibited an obvious one-dimensional structure with diameters of 150–200 nm and lengths of 400–500 nm. The markedly increased aspect ratio of nanorods can be in the range of 1.5–3. If the ZnO was grown in the electrolyte with 1.0 % PVP (sample S3), as shown in Fig. 5d, the number of ZnO nanorods grown on the porous silicon decreased significantly. The significantly enlarged ZnO nanorods with diameters of 200–300 nm and lengths of 600–1000 nm sparsely scattered on the surface of the PS. The aspect ratio of nanorods can be in the range of 3–5. In a word, all the products (sample S1, S2, and S3) showed a dendritic structure; the higher the concentration of PVP, the bigger the aspect ratio of the ZnO nanorods. In other words, the use of PVP in the electrolyte can effectively promote the vertical growth of ZnO crystals and disperse the nucleation of ZnO nanorods [31].

The mechanisms of electrochemical synthesis ZnO nanorods [22] is proposed as the reduction of dissolved molecular oxygen in zinc chloride solutions by a two (Eq. (1)) or a four (Eq. (2)) electron process.

$$O_2 + 2H_2O + 2e^- \rightarrow H_2O_2 + 2OH^- \quad (1)$$

$$O_2 + 2H_2O + 4e^- \rightarrow 4OH^- \quad (2)$$

$$Zn^{2+} + 2OH^- \rightarrow ZnO + H_2O \quad (3)$$

The hydroxide ions generated from the reaction induces an increase of the local pH close to the cathode. Zn^{2+} and OH^- ions react together to form zinc oxide which deposited at the surface of the PS (Eq. (3)). The initial stage of crystal growth is without direction selectivity. The PVP in the solution will

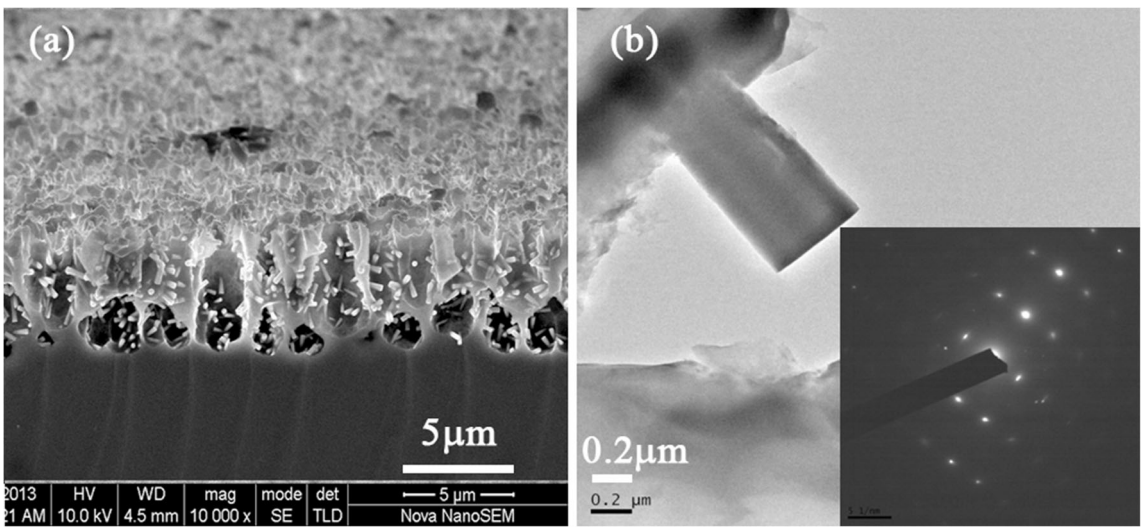

Fig. 6 **a**–**b** The cross-sectional SEM images of the ZnO nanorods/PS (sample S3) and the TEM image of the ZnO nanorods/PS (sample S2). The inset in (**b**) is the SAED pattern of the corresponding product

not participate in the electrochemical reaction, but adsorb onto the ZnO facets through chemical interactions.

Some researchers [32, 33] have found that polymers may have different surface interaction strengths with the atoms on different crystallographic facets, leading to the anisotropic growth of a crystalline material. Liu et al. [23, 31] study the role of PVP in the cathodic electrodeposition ZnO from oxygenated zinc chloride aqueous solution. They think that owing to the more surface defects of the high index crystal planes (side facets of hexagonal ZnO columns) than the low-index crystal plane (end facets of hexagonal ZnO columns), PVP interacts more strongly with the side facets than with the end facets of hexagonal ZnO nanorods. Therefore, the side facets of ZnO nanorods absorb more PVP than the end side facets. In other words, PVP plays a passivation effect on the side facets of ZnO crystals, which inhibits the growth of side facets and meanwhile protects the regularity of the side facets. The uncovered end face of ZnO crystals remain active to the freshly reducing ZnO molecules and subsequent growth on end facets results in the formation of ZnO hexagonal nanorods. Briefly, the passivation PVP forms on the surface of side facets lead to the anisotropic growth of ZnO nanorods. It can selectively promote vertical growth while inhibit lateral growth of ZnO crystals [23, 31].

Although with different aspect ratio, the nanorods in the three samples were short in contrast to the diameter of porous silicon. For all the samples, the pore structure of porous silicon revealed.

From the cross-sectional view of the ZnO nanorods/PS (sample S3) in Fig. 6a, it can be seen that straight, smooth, hexagonal prisms were grown inside the silicon pore, until the hole bottom which indicated a relatively uniform electric field distribution inside the whole hole in the electrodeposition process. The TEM image and the SAED pattern of the ZnO nanorods/PS composite (sample S2) in Fig. 6b further evidenced that the nanocrystalline ZnO grow on the hole-wall of PS.

The XRD pattern of the ZnO nanorods/PS (samples S2) was shown in Fig. 7. The XRD patterns of other samples were similar to it. All the peaks can be indexed well to the wurtzite ZnO phase (JCPDS Card no. 36-1451). The XRD intensity distribution of the three samples is similar to the standard pattern of ZnO crystal, indicating that the nanorods were orientated randomly, consistent with the SEM images.

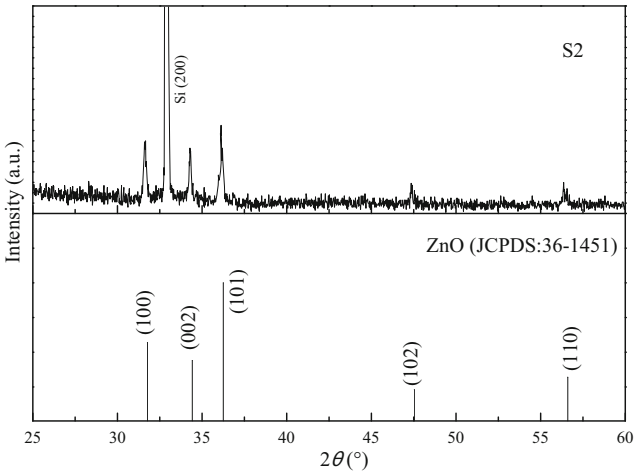

Fig. 7 XRD patterns of ZnO nanorods/PS: sample S2 (*vertical lines*: JCPDS no. 36-1451)

NO_2-sensing properties

Figure 8 illustrated the relationship between the sensor sensitivities of four sensors and operating temperature. As can be seen from Fig. 8, all the sensors have the same response trend that the sensitivities of all the sensors decreased continuously as the temperature increases. It means that all the sensors had the same operating temperature (RT), which is different from the typical zinc oxide-based sensor with the high operating temperature but consistent with typical PS-based sensor with a RT operating temperature [10, 26]. In addition, the morphology of the ZnO nanorods/PS composite plays a vital role in determining the NO_2-sensing properties. For all the sensors, the more densely nanorods grown on porous silicon, the bigger aspect ratio of the nanorods was, the better the gas-sensing performance of the sample has. Because the growth and the nucleation of ZnO nanorods were modulated by the PVP in the electrolyte, the gas-sensing properties of the sensors were related to the PVP concentration of the electrolyte. The sensor sensitivities increase with increasing the PVP concentration at first, attain a maximum value, and then decrease with the further increase of the PVP concentration. So the sensitivities of the sensor(sample S2) grown from the electrolyte with the PVP mass ratios of 0.5 % were marked higher than those

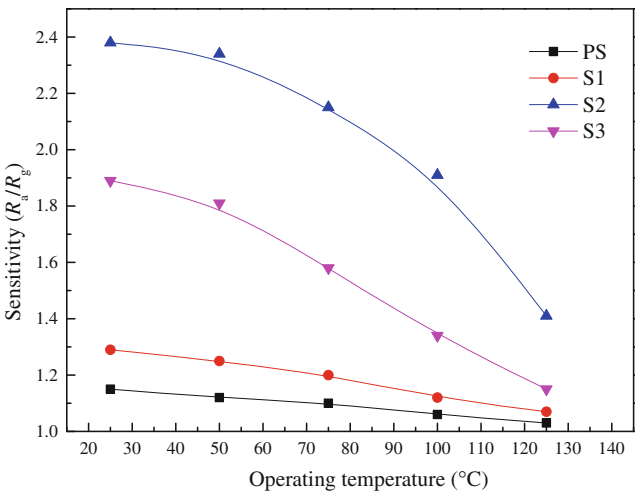

Fig. 8 The sensitivities of four sensors to 1 ppm NO_2 as a function of operating temperature

of other sensors (sample S1 and sample S3) in the whole temperature range from 25 °C (RT) to 125 °C. In addition, the sensitivities of sample S3 were higher than sample S1 and the sample PS had the minimum value of the sensitivities in the whole temperature range.

Figure 9 shows the dynamic responses of the three sensors (samples PS, S1, S2, and S3) in various NO_2 gas concentrations (100 ppb to 1 ppm) at the operating temperature 25 °C (RT). According to the definition of response, the electrical resistance of all the sensors decreases upon exposure to NO_2, which is contrary to the typical n-type zinc oxide-based sensor but consistent with typical tendency of p-type PS towards oxidizing gases [10, 34]. It means that the ZnO nanorods/PS composite sensor exhibits a typical p-type semiconductor gas-sensing behavior. Moreover, the ZnO nanorods/PS composite sensor exhibits higher sensitivity to NO_2 than that of pure macro-PS. In addition, it can also be seen from Fig. 9 that the response of PS to NO_2 is almost irreversible, while the resistance of the ZnO nanorods/PS sensor (samples S2) decreases dramatically upon exposure to NO_2 and restores to its original value upon exposure to air at RT. The present study indicates the sensor (samples S2) has a good response and recovery performance.

Figure 10 represents the relationships between NO_2 concentrations and sensor sensitivities of different sensors at RT. It is clear that the sensor sensitivities increase nearly linearly with increasing of the NO_2 gas concentration in the range of 100 to 400 ppb. Above 400 ppb, the sensitivities rising speed descend slightly, which indicates that the sensor response becomes more or less saturated. Moreover, the sample with more slender nanorods (sample S2) exhibits the highest response compared to the sample with less nanorods (sample S3) and the sample with thick nanorods (sample S1). The gas-sensing response of sample S1 is close to that of the sample PS. That is to say, the slender ZnO nanorods significantly improve the NO_2-sensing response of PS, but the thick ZnO nanorods have little effect to the gas-sensing response of PS.

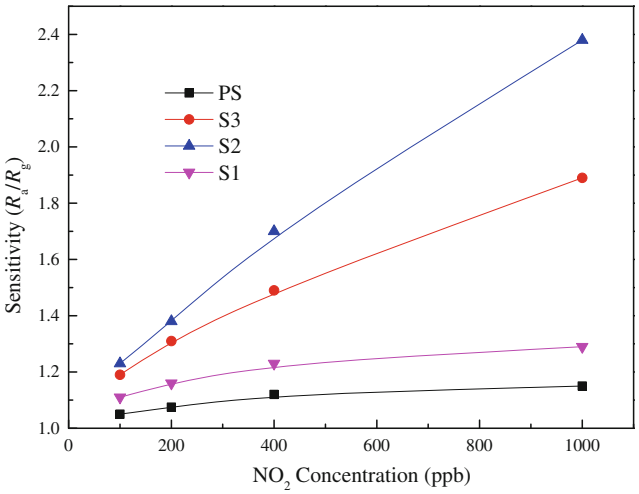

Fig. 10 Relationship between the sensor sensitivities and NO_2 concentration for different sensors at RT

The repeatability and selectivity are important considerations for the practical application of gas sensor. Figure 11 showed the dynamic response of the sensor (sample S2) to four representative cyclic exposures of 1 ppm NO_2 gas at RT. From Fig. 11, it can be seen the sensor has a similar response value and response-recovery time for each test. Notably, it indicated the sensor (sample S2) had an excellent repeatability and stability. A comparison between the sensitivities of the sensor (sample S2) for different gases at RT was shown in Fig. 12. Apparently, the sensor exhibits a good selectivity to NO_2 gas.

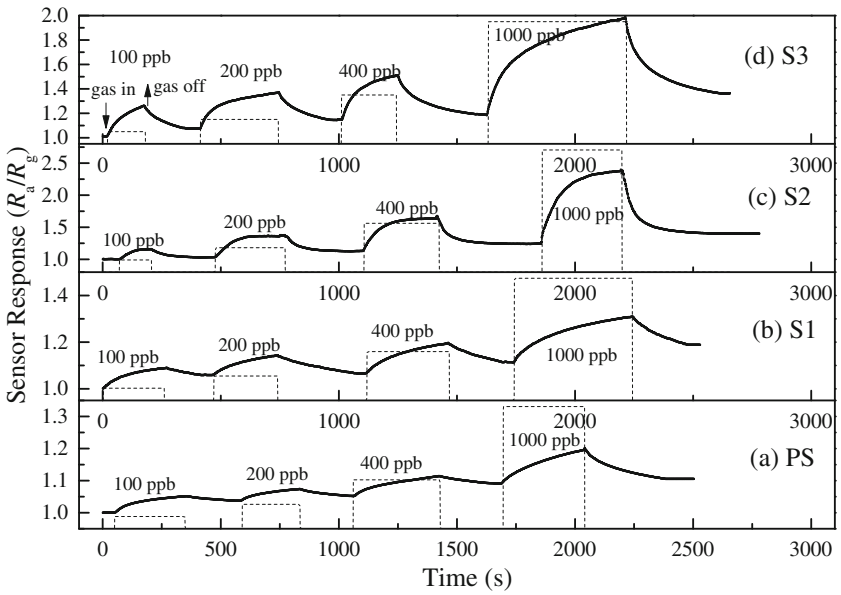

Fig. 9 **a**–**d** Dynamic responses of the sensors (sample PS, S1, S2, and S3) to various concentration of NO_2 at RT

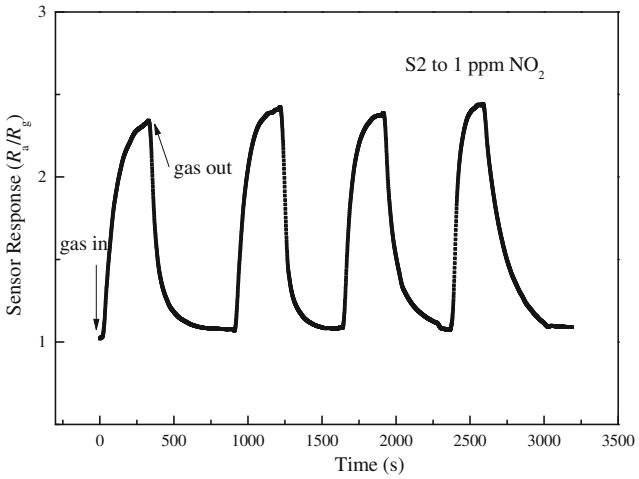

Fig. 11 Dynamic response of ZnO nanorods/PS sensor (sample S2) as a function of time for four cycles to 1 ppm of NO_2 at RT

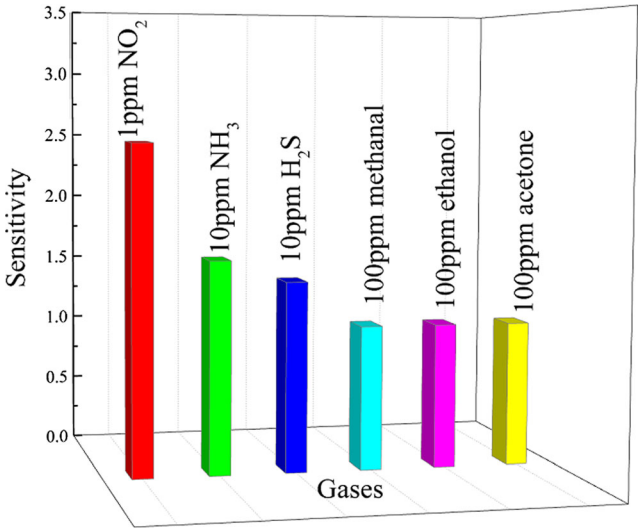

Fig. 12 Sensor sensitivities of the ZnO nanorods/PS sensor (sample S2) to various gases at RT

Gas-sensing mechanisms

The gas-sensing mechanism of the ZnO nanorods/PS composite sensor was taken into consideration.

Figure 13a shows a structure diagram of the ZnO nanorods/PS gas sensor, which indicates that the heterojunction effect plays an important role for the gas-sensing mechanism of the ZnO nanorods/PS sensor.

As a component of the ZnO nanorods/PS composite, the PS is gas sensitive based on surface-controlled model [35]. When the p-type PS is exposed to the air independently, the exposed surface of PS adsorbs the oxygen molecules from the air, which extract electrons from the conduction band and formO^-, O_2^-, and O^{2-} [36, 37]. As a result, the electron-depleted space-charge layers in the surface of PS are formed. When the PS is exposed to the strong oxidizing gases NO_2 independently, the NO_2 molecules may be directly adsorbed onto the surfaces of PS by trapping electrons and reacting with the surface adsorbed speciesO^-, O_2^-, and O^{2-} [36, 37]. The reaction will decrease further the thickness of the space-charge layer of the PS surface, accordingly increasing the conducting channel width of the holes in the PS surface. Therefore, the resistance of the PS (R_{PS}) will decrease when PS is exposed to the NO_2 independently. The corresponding schematic diagram was shown in Fig. 13b. This is the mechanism that explains why nitrogen dioxide can be detected by PS at room temperature (Fig. 9a).

Similarly, as the other component of the ZnO nanorods/PS composite, the ZnO nanorods are gas sensitive based on the coaxial cable model [38]. ZnO was an n-type semiconductor with the majority carriers of electrons because the oxygen vacancies in ZnO serve as electron donors. Thus, when the ZnO nanorods are exposed to the air independently, some oxygen molecules in the air will be adsorbed on the surface of ZnO nanorods and capture electrons from the conduction band to formO^-, O_2^-, and O^{2-} [39, 40]. Then the depletion layer was formed on the surface regions of nanorods, just like a coaxial cable (Fig. 13c), which reduced the carrier concentration. When the ZnO nanorods are exposed to strong oxidizing gases NO_2 independently, the gas will react with the adsorbedO^-, O_2^- andO^{2-} and capture the electrons from the conduction band further [39, 40]. The reaction will decrease the conducting channel width of the electrons in the ZnO nanorods surface. Therefore, the resistance of the ZnO nanorods (R_{ZnO}) will increase when ZnO nanorods are exposed to the NO_2 independently.

Given the fact that the ZnO nanorods were grown onto the surface of PS, if the gas-sensing properties of the composite were simply an addition of the performance of each component, the sensitivities of the composite should be less than the pure PS, but testing showed otherwise. Therefore, we assume the gas-sensing properties of the ZnO nanorods/PS composite sensor, on the basis of gas-sensing characteristics of each component, are the comprehensive performance produced by the heterojunction effect among each the components.

Considering the ZnO nanorods growing on the hole-wall of PS to form a dendritic structure, the ZnO nanorods and the PS in the heterojunction have different status in the circuit structure of the sensor. When the current flows through the sensor, PS is the main channel rather than ZnO nanorods, as shown in Fig. 13b. Upon exposure to NO_2, not only the electrons of PS were captured but also the electrons of ZnO nanorods were trapped simultaneously. The latter in turn causes an effective electronic transfer from the PS towards the ZnO nanorods. Once again the electron transfer of the heterojunction results in a rapid decrease of the sensor resistance. Figure 13d shows the heterojunction effect schematic diagram of the NO_2-sensing mechanisms and the energy band diagram of the ZnO nanorods/PS composite, where ZnO has a larger band gap

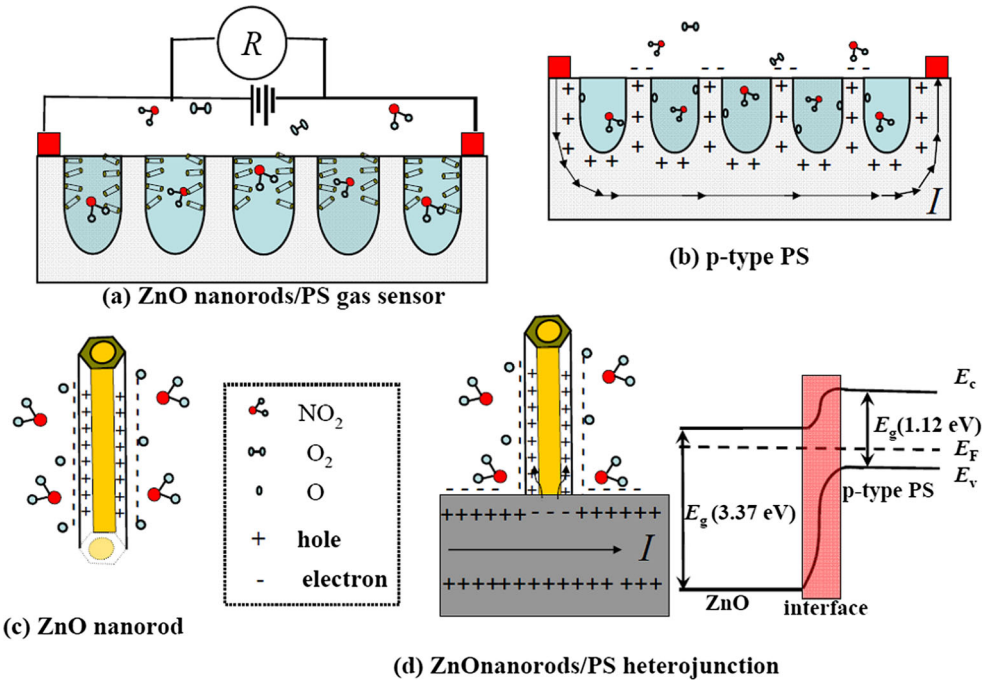

Fig. 13 The schematic diagram of gas-sensing mechanisms for the ZnO nanorods/PS sensor to NO_2. **a** the structure diagram of the ZnO nanorods/PS gas sensor. **b** the NO_2-sensing mechanisms for the p-type PS independently. **c** the NO_2-sensing mechanisms for the ZnO nanorods independently. **d** the heterojunction effect in the NO_2-sensing mechanisms and the energy band diagram of the ZnO nanorods/PS composite

(about 3.37 eV) than that of PS (about 1.12 eV). An electron depletion layer or potential barrier is formed and the energy band bends at the interface. The heterojunction effect may be responsible for the fact that the composite sensor is more responsive than the PS gas sensor.

In addition, the sample with more ZnO nanorods and a larger aspect ratio of ZnO nanorods results in a larger surface area, which induce the high surface energy. Therefore, the surface is much more active and can provide more adsorption site for the gas molecules. More electrons will transfer from the PS towards the ZnO nanorods when the corresponding ZnO nanorods/PS sample was exposed to NO_2. Thus, sample S2 with more thin nanorods have a significantly better sensing performance than samples S1 and S3.

Intuitively, the good response-recovery performance of the ZnO nanorods/PS sensor is related to the uniformly densely aligned pore channels of PS, which is beneficial to the diffusion of gas molecules.

Besides, the relevant studies [41] have shown that the deposition of ZnO on the porous silicon leads to the cleavage of the Si–H bonds and formation the Si–O bands. We assume the change of surface state and the passivation effect [26, 41] may be responsible for the improvement of repeatability and selectivity.

Conclusions

In this work, ZnO nanorods with different aspect ratio were electrodeposited onto PS with addition of different contents of PVP into the electrolyte based on zinc chloride aqueous solution. SEM images, TEM images, and the XRD pattern confirmed the formation of wurtzite ZnO nanorods on the PS and give evidences that PVP added into the electrolyte can selectively promote the growth in the vertical direction of the ZnO crystals. The gas-sensing tests indicated the composite sensor with larger aspect ratio and denser ZnO nanorods exhibited good gas-sensing performances to NO_2 gas, including high response value, fast response-recovery characteristics, good repeatability and selectivity, as well as the low optimal operating temperature of RT due to the high specific surface area and special structural and morphological properties. The result of the gas-sensing mechanism analysis indicates the heterojunction effect between the ZnO and PS may play an important role in the gas-sensing mechanisms. The results show excellent potential applications in NO_2 sensor which favor low power consumption, high sensitivity, and integration technology.

Acknowledgments This project is supported by the National Natural Science Foundation of China (Nos. 61474082 and 11104203) and the Tianjin Normal University Doctoral Foundation of China (No. 52XB1416).

References

1. Qin Y, Sun X, Li X, Hu M (2012) Room temperature NO_2-sensing properties of Ti-added nonstoichiometric tungsten oxide nanowires. Sensor Actuat B-Chem 162:244–250
2. Zeng J, Hu M, Wang W, Chen H, Qin Y (2012) NO_2-sensing properties of porous WO_3 gas sensor based on anodized sputtered tungsten thin film. Sensor Actuat B-Chem 161:447–452

3. Pasierb P, Rekas M (2009) Solid-state potentiometric gas sensors—current status and future trends. J Solid State Electr 13:3–25
4. Möbius HH, Hartung R (2010) Solid-state potentiometric gas sensors—a supplement. J Solid State Electr 14:669–673
5. Kim SJ, Jeon BH, Choi KS, Min NK (2000) Capacitive porous silicon sensors for measurement of low alcohol gas concentration at room temperature. J Solid State Electr 4:363–366
6. Rheaume JM, Pisano AP (2012) Investigation of an impedancemetric NO_x sensor with gold wire working electrodes. J Solid State Electr 16:3603–3610
7. Ahmad MZ, Chang J, Ahmad MS, Waclawik ER, Wlodarski W (2013) Non-aqueous synthesis of hexagonal ZnO nanopyramids: gas sensing properties. Sensor Actuat B-Chem 177:286–294
8. Li C, Gao M, Ding C, Zhang X, Zhang L, Chen Q, Peng LM (2009) In situ comprehensive characterization of optoelectronic nanomaterials for device purposes. Nanotechnology 20:175703
9. Bahadur L, Kushwaha S (2013) Structural and optical properties of tripod-like ZnO thin film and its application in dye-sensitized solar cell. J Solid State Electr 17:2001–2008
10. Öztürk S, Kılınç N, Taşaltin N, Öztürk ZZ (2011) A comparative study on the NO_2 gas sensing properties of ZnO thin films, nanowires and nanorods. Thin Solid Films 520:932–938
11. Sadek AZ, Choopun S, Wlodarski W, Ippolito SJ, Kalantar-zadeh K (2007) Characterization of ZnO nanobelt-based gas sensor for H_2, NO_2, and hydrocarbon sensing. IEEE Sensors J 7:919–924
12. Li J, Fan H, Jia X (2010) Multilayered ZnO nanosheets with 3D porous architectures: synthesis and gas sensing application. J Phys Chem C 114:14684–14691
13. Rai P, Raj S, Ko K, Park K, Yu Y (2013) Synthesis of flower-like ZnO microstructures for gas sensor applications. Sensor Actuat B-Chem 178:107–112
14. Han X, He H, Kuang Q, Zhou X, Zhang X, Xu T, Xie Z, Zheng L (2009) Controlling morphologies and tuning the related properties of nano/microstructured ZnO crystallites. J Phys Chem C 113:584–589
15. Liao L, Lu HB, Li JC, He H, Wang DF, Fu DJ, Liu C, Zhang WF (2007) Size dependence of gas sensitivity of ZnO nanorods. J Phys Chem C 111:1900–1903
16. Ahn MW, Park KS, Heo JH, Park JG, Kim DW, Choi KJ, Lee JH, Hong SH (2008) Gas sensing properties of defect-controlled ZnO-nanowire gas sensor. Appl Phys Lett 93:263103
17. Fang F, Zhao DX, Zhang JY, Shen DZ, Lu YM, Fan XW, Li BH, Wang XH (2007) Growth of well-aligned ZnO nanowire arrays on Si substrate. Nanotechnology 18:235604
18. Wang JX, Sun XW, Yang Y, Wu CM (2009) N-P transition sensing behaviors of ZnO nanotubes exposed to NO2 gas. Nanotechnology 20:465501
19. Cao X, Wang N, Wang L (2010) Ultrathin ZnO nanorods: facile synthesis, characterization and optical properties. Nanotechnology 21:65603
20. Kitazawa N, Aono M, Watanabe Y (2014) Growth of vertically aligned one-dimensional ZnO nanowire arrays on sol-gel derived ZnO thin films. J Phys Chem Solids 75:1194–1200
21. Gomez H, Riveros G, Ramirez D, Henriquez R, Schrebler R, Marotti R, Dalchiele E (2012) Growth and characterization of ZnO nanowire arrays electrodeposited into anodic alumina templates in DMSO solution. J Solid State Electr 16:197–204
22. Elias J, Tena-Zaera R, Lévy-Clément C (2008) Electrochemical deposition of ZnO nanowire arrays with tailored dimensions. J Electroanal Chem 621:171–177
23. Liu YL, Liu YC, Feng W, Zhang JY, Lu YM, Shen DZ, Fan XW, Wang DJ, Zhao QD (2005) The optical properties of ZnO hexagonal prisms grown from poly(vinylpyrrolidone)-assisted electrochemical assembly onto Si (111) substrate. J Chem Phys 122:174703
24. Razi F, Rahimi F, Iraji Zad A (2008) Fourier transform infrared spectroscopy and scanning tunneling spectroscopy of porous silicon in the presence of methanol. Sensor Actuat B-Chem 132:40–44
25. Ozdemir S, Gole JL (2010) A phosphine detection matrix using nanostructure modified porous silicon gas sensors. Sensor Actuat B-Chem 151:274–280
26. Ali NK, Hashim MR, Aziz AA (2008) Effects of surface passivation in porous silicon as H_2 gas sensor. Solid State Electron 52:1071–1074
27. Kanungo J, Saha H, Basu S (2010) Pd sensitized porous silicon hydrogen sensor—influence of ZnO thin film. Sensor Actuat B-Chem 147:128–136
28. Ma S, Hu M, Zeng P, Li M, Yan W, Qin Y (2014) Synthesis and low-temperature gas sensing properties of tungsten oxide nanowires/porous silicon composite. Sensor Actuat B-Chem 192:341–349
29. Li MD, Hu M, Zeng P, Ma SY, Yan WJ, Qin YX (2013) Effect of etching current density on microstructure and NH_3-sensing properties of porous silicon with intermediate-sized pores. Electrochim Acta 108:167–174
30. Mareš J, Krištofik J, Hulicius E (1995) Influence of humidity on transport in porous silicon. Thin Solid Films 255:272–275
31. Liu Y, Liu Y, Zhang J, Lu Y, Shen D, Fan X (2006) ZnO hexagonal prisms grown onto p-Si (111) substrate from poly (vinylpyrrolidone) assisted electrochemical assembly. J Cryst Growth 290:405–409
32. Ahmadi TS, Wang ZL, Green TC, Henglein A, El-Sayed MA (1996) Shape-controlled synthesis of colloidal platinum nanoparticles. Science 272:1924–1926
33. Sun YG, Mayers B, Herricks T, Xia YN (2003) Polyol synthesis of uniform silver nanowires: a plausible growth mechanism and the supporting evidence. Nano Lett 3:955–960
34. Wu Y, Hu M, Qin Y, Wei X, Ma S, Yan D (2014) Enhanced response characteristics of p-porous silicon (substrate)/p-TeO_2 (nanowires) sensor for NO_2 detection. Sensor Actuat B-Chem 195:181–188
35. Mizsei J (1995) How can sensitive and selective semiconductor gas sensors be made? Sensor Actuat B-Chem 23:173–176
36. Li M, Hu M, Jia D, Ma S, Yan W (2013) NO_2-sensing properties based on the nanocomposite of n-WO_{3-x}/n-porous silicon at room temperature. Sensor Actuat B-Chem 186:140–147
37. Li M, Hu M, Liu Q, Ma S, Sun P (2013) Microstructure characterization and NO_2-sensing properties of porous silicon with intermediate pore size. Appl Surf Sci 268:188–194
38. Lupan O, Ursaki VV, Chai G, Chow L, Emelchenko GA, Tiginyanu IM, Gruzintsev AN, Redkin AN (2010) Selective hydrogen gas nanosensor using individual ZnO nanowire with fast response at room temperature. Sensor Actuat B-Chem 144:56–66
39. Bai SL, Hu JW, Xu XY, Luo RX, Li DQ, Chen AF, Liu CC (2012) Gas sensing properties of quantum-sized ZnO nanoparticles for NO_2. IEEE Sensors J 12:1234–1238
40. Rai P, Yu YT (2012) Citrate-assisted hydrothermal synthesis of single crystalline ZnO nanoparticles for gas sensor application. Sensor Actuat B-Chem 173:58–65
41. Wu XL, Xiong SJ, Fan DL, Gu Y, Bao XM, Siu GG, Stokes MJ (2000) Stabilized electronic state and its luminescence at the surface of oxygen-passivated porous silicon. Phys Rev B 62:R7759–R7762